J Phys. B: At. Mol. Opt. Phys. **28** (1995) 3163–3183. Printed in the UK

Highly doubly excited S states of the helium atom

Andre Bürgers†, Dieter Wintgen and Jan–Michael Rost
Fakultät für Physik, Universität Freiburg, Hermann-Herder-Str. 3, 79104 Freiburg, Germany

Received 23 March 1995

Abstract. We calculate and analyse S-wave resonances of helium up to an energy of -0.02 au applying the complex rotation technique. Rydberg series converging to the hydrogenic thresholds of the He^+ ion are analysed by quantum defect theory. For moderately excited inner electrons the series converging to different thresholds begin to overlap resulting in perturbed Rydberg series. We find that approximate quantum numbers as well as propensity rules governing the decay of the resonances and the perturbation scheme of the Rydberg series prevail. With increasing excitation of the inner electron however, only series whose states tend to extreme interelectronic angles $(\cos\theta) = \pm 1$ remain regular.

1. Introduction

Since the first experiment by Madden and Codling (1963) doubly excited states of helium have attracted the interest of theoreticians and experimentalists. Recent experiments study with high resolution the photoabsorption of helium to doubly excited states (Domke *et al* 1991, 1992, 1995). Numerous theoretical investigations have improved our understanding of the electron–electron correlation which prevents an analytical solution for the helium atom. The classification of isolated resonances according to approximate quantum numbers is now well established and has emerged from different approaches (Herrick 1983, Lin 1986, Feagin and Briggs 1986). The classification is accompanied by propensity rules which govern the autoionization pattern of the resonances (Rost and Briggs 1990). Hence the low and intermediate lying region appears to be well understood and highly accurate *ab initio* calculations are available.

Various methods have been applied to obtain the resonance parameters theoretically. Bathia and Temkin (1975, 1984) used a Feshbach projection formalism whereas a close coupling approximation was employed by Oza (1986). The multi-configurational Hartree–Fock method was extended to autoionizing states by Froese-Fischer and Indrees (1990), and Tang *et al* (1992) used a hyperspherical close coupling method based on a numerical basis set. Müller *et al* (1994) applied the stabilization method of Mandelshtam *et al* (1993) to calculate $^1S^e$ states of helium. The *complex rotation* technique, which is also used in this work, makes it possible to use bound state methods to calculate autoionizing states. This method was extensively used by Ho and co-workers (1979, 1980, 1981, 1983, 1986) with a Hylleraas-type basis set. Lindroth (1994) applied the complex rotation method with a finite numerical basis set built on solutions of the discretized one-particle Hamiltonian (Salomonson and Öster 1989).

More recently interest has shifted to very high excitation and to the question whether the approximate quantum numbers and propensity rules prevail up to the fragmentation

† E-mail address: andre@phyc1.physik.uni-freiburg.de

0953-4075/95/153163+21$19.50

threshold $E = 0$ of helium. For this purpose the present work supplies very accurate numerical data for high excitation of both electrons with principal quantum numbers of the inner (N) and outer (n) electron up to $n \geqslant N = 10$.

The accuracy and the large amount of our data allows us to analyse the spectrum of the S states of helium up to energies where series converging to different thresholds of the He^+ ion strongly overlap. Using a quantum defect analysis (Seaton 1983, Wintgen and Friedrich 1987) we are able to identify deviations from the regular Rydberg behaviour very clearly. For moderate excitation, autoionization transitions obey the propensity rules derived by Rost and Briggs (1990, 1991) in the molecular orbital description of the He atom. We find that these propensity rules break down for very highly doubly excited states far from the quasi-classical regime.

Surprisingly, however, this does not imply a change in the autoionization mechanism on which the propensity rules are based. On the contrary this mechanism together with the so called perturber states (to be defined later) can be used to show that most Rydberg series are strongly mixed with respect to the channels defined by the approximate quantum numbers. Since the propensity rules connect just these 'pure' channels, their violation for highly excited Rydberg series indicates that these states are no longer built of pure channels but of mixtures of those. We will discuss the evolution of the channel mixing as a function of excitation energy in detail. We will also relate our results to recent semiclassical descriptions of the two–electron atom (Ezra *et al* 1991, Richter and Wintgen 1991, Richter *et al* 1992, Müller *et al* 1992).

The paper is organized as follows. In section 2 we present the Hamiltonian of the problem in the coordinates we use and discuss our method of solution. As an example for the accuracy we achieve we present some energies of singly excited states. Section 3 deals with the tools used to classify and analyse doubly excited resonances. Approximate quantum numbers (for the classification) and some aspects of quantum defect theory (for the analysis) are briefly discussed. In section 4 we present our results for the resonance spectrum of helium in detail with an emphasis on singlet states. Some examples for triplet Rydberg series are also reported to illustrate the qualitative similarity between singlet and triplet series. Section 5 contains the summary and conclusion.

2. Hamiltonian in perimetric coordinates and method of solution

2.1. Analytic matrix representation of the Hamiltonian

The non-relativistic Hamiltonian for the relative motion of a two-electron atom or ion with nuclear charge Z reads (atomic units are used throughout the paper)

$$H = -\frac{\nabla_1^2}{2} - \frac{\nabla_2^2}{2} - \frac{Z}{r_1} - \frac{Z}{r_2} + \frac{1}{r_{12}}. \tag{1}$$

Here, ∇_1 and ∇_2 are the momentum operators in position representation, r_1 and r_2 the distances of the electrons from the nucleus, and $r_{12} = |r_1 - r_2|$ is the inter-electronic distance. The mass of the nucleus is assumed to be infinite.

The wavefunction of the two-electron system is conveniently written as (Breit 1930, Wintgen and Delande 1993, Pont and Shakeshaft 1995)

$$\Psi_{LM}(r_1, r_2) = \sum_{-L \leqslant M' \leqslant L} \mathcal{D}^L_{MM'}{}^*(\psi, \theta, \phi)\Phi_{M'}(r_1, r_2, r_{12}), \tag{2}$$

where the $\mathcal{D}^L_{MM'}(\psi, \theta, \phi)$ are the rigid-top wavefunctions describing the rotation from a laboratory frame to a body fixed frame with the Euler angles ψ, θ, ϕ. In this paper we

restrict ourselves to $L = 0$ states for which the dynamics in the plane spanned by the three particles does not depend on its orientation in space. Hence we can restrict our considerations to this plane described by three variables only. Formally this corresponds to $\mathcal{D}^0_{00} =$ constant in (2).

The full solution of the corresponding Schrödinger equation remains nevertheless a nontrivial problem. We use a transformation of the Schrödinger equation to perimetric coordinates as defined by Coolidge and James (1937). Even though this coordinate set has already been used for numerical ground state calculations as early as 1958 (Pekeris), its power and simplicity for the calculation of highly doubly excited states was not fully recognized in the past. The perimetric coordinates have the great advantage that they produce, together with an appropriately chosen basis set, a matrix representation of the hamiltonian which is sparse and of banded structure and therefore allows for an efficient diagonalization. The perimetric coordinates are defined as follows:

$$\begin{aligned} x &= r_1 + r_2 - r_{12} \\ y &= r_1 - r_2 + r_{12} \qquad x, y, z \geqslant 0 . \\ z &= -r_1 + r_2 + r_{12} \end{aligned} \tag{3}$$

In these coordinates the Hamiltonian (1) reads

$$H = \sum_{i,j=x,y,z} \partial_i^{\dagger} \frac{P^{(3)}_{ij}(x, y, z)}{(x+y)(x+z)(y+z)} \partial_j - \frac{2Z}{x+y} - \frac{2Z}{x+z} + \frac{2}{y+z} . \tag{4}$$

The $P^{(3)}_{ij}$ in (4) are polynomials of degree 3 of the variables x, y, z and can be found in the appendix. (The dagger with the partial derivative in (4) means that this operator acts to the left.)

We expand the wavefunction for each degree of freedom in a complete Sturmian basis set and (anti-) symmetrize the product functions (the exchange of the two electrons corresponds to an exchange of the y and z coordinates). An element of this basis then reads

$$\Phi^{\pm}_{nmk}(x, y, z) = \phi_n(\alpha x)\left[\phi_m(\beta y)\phi_k(\gamma z) \pm \phi_k(\gamma y)\phi_m(\beta z)\right] \tag{5}$$

with $\phi_n(u)$ defined as

$$\phi_n(u) = L_n(u)\, \mathrm{e}^{-u/2} \tag{6}$$

where the $L_n(u)$ are the usual Laguerre polynomials. The volume element

$$\mathrm{d}V = \frac{8\pi^2}{32}(x+y)(x+z)(y+z)\,\mathrm{d}x, \mathrm{d}y, \mathrm{d}z \tag{7}$$

cancels the singularities in the Hamiltonian (4) if matrix elements are calculated. Orthonormalization and recursion relations of the Laguerre polynomials guarantee that most of the matrix elements between basis states vanish. This leads to the sparse and (under appropriate order of the basis elements) banded structure of the matrix representation of the Hamiltonian. The calculation of the non-vanishing matrix elements is simple and can be done algebraically using fast and accurate integer arithmetic.

The eigenvalues of the matrix do not depend on the parameters α, β, γ in (5) if a complete basis is used. In numerical calculations, however, only a finite basis can be implemented on the computer because of limited storage capacities. We use truncated basis sets up to a maximum node number $\omega = n + m + k = 64$, corresponding to 24 497 basis states. The convergence is checked with respect to increasing basis size. This convergence, however, is sensitive to the choice of our scaling parameters α, β, γ. We rewrite them as $\alpha = a\beta$ and $\gamma = c\beta$ and choose a and c to be real. For states where both electrons

are approximately symmetrically excited, $c = 1$ is the natural choice. This leads to a further reduction of the bandwidth of the matrix since there are even more matrix elements exactly vanishing due to the orthonormalization relations of the Laguerre polynomials. For asymmetrically excited states, c should be approximately equal to the quotient of the principal hydrogenic quantum numbers of the two electrons in the independent-electron limit to obtain a rapid convergence. However, in this case the bandwidth is significantly larger than in the $c \approx 1$ case, which not only increases the computation time but also lowers the maximum basis size that can be implemented under the same storage capacities ($\omega = 42$ instead of 64). Hence we have used $c \neq 1$ only for moderately excited states. A good choice for a is $a = 1 + c$ which gives the correct asymptotic behaviour in the independent-electron limit.

With these parameters the Schrödinger equation (4) has the matrix form

$$(\beta^2 \hat{T} + \beta \hat{V} - E\hat{N})\Psi = 0. \tag{8}$$

The matrices $\hat{T}, \hat{V}, \hat{N}$ of the kinetic energy T, the potential energy V and the unit operator N are real symmetric and depend on a and c, but *not* on β.

For real β the matrix equation (8) represents a real variational problem leading to real eigenenergies of the hamiltonian. Hence, with real β the real energies of singly excited states can be calculated. Resonances, however, are described by complex energies,

$$E_{\text{res}} = E_R - i\Gamma/2. \tag{9}$$

To calculate those complex energies, we apply the complex rotation technique (Reinhardt 1982, Ho 1983). It is implemented by using a *complex* variational parameter β in (8),

$$\beta = be^{i\vartheta} \tag{10}$$

with real b, ϑ. A typical choice for b is $b = 1/N$ or smaller (N is the principal quantum number of the He^+ ion to which the Rydberg series converges).

By solving (8) we get a large number of converged complex eigenvalues that represent the doubly excited resonances.

2.2. *Numerical computation of resonances*

The actual computation of the eigenvalues of (8) is performed in two steps. In a first step a certain number of eigenvalues is calculated around a (complex) energy by using a fast Lanczos algorithm (Delande *et al* 1991). In this way we get a number of candidates with one program call. The eigenvalues are checked for convergence by systematically increasing the basis size. Note that at this stage the parameter β is not optimized but remains the same for all eigenvalues calculated at the same time.

In a second step the complex matrix equation (8) is solved using an inverse iteration method on an LDL^T decomposition of the matrix (8) with the results from step one as starting values. This program also calculates some expectation values, using the expansion coefficients of the eigenstate in the basis set. For each state we use an iterative algorithm to optimize the complex scaling parameter β such that the complex energy becomes stationary, $\partial E/\partial\beta = 0$. The wavefunction then fulfils the complex virial theorem $-2\langle T\rangle = \langle V\rangle = 2E$ (Ho 1983). Here we also check the convergence of the complex eigenvalues with respect to the basis size and the partial derivative $\partial E/\partial a$, which should also vanish for an exact eigenfunction. It turns out that most of the (well converged) eigenvalues obtained by the Lanczos algorithm fulfil the specified accuracy after only a few (sometimes only one) iterations so that in most cases the results of our first step are good enough if one is only

interested in the resonance energies. This can be interpreted as a signature of a weak dependence of the energy on β for large basis sets.

2.3. Accuracy

To demonstrate the accuracy of this method we list here our results for the energies of singlet and triplet singly excited states of the He atom (table 1). All converged digits are shown. The numbers in parentheses give the maximum uncertainty in the last digit(s). For comparison, we show (in italics) the hitherto most accurate data we are aware of (Drake 1988).

The energies for doubly excited states can be calculated as accurately as for moderately singly excited states. In the following we will present our resonance energies with an accuracy of 10^{-9} au although most of the data are better converged. In the worst cases the uncertainty is not larger than 2 in the last digit quoted.

Table 1. Energies of the singly excited Rydberg series labeled by independent electron quantum numbers. The numbers in italics are the results obtained by Drake (1988) using a set of Hylleraas type basis functions. The numbers in parentheses denote the accuracy in the last digit(s).

state	$-E(^1S)$	$-E(^3S)$
1s1s	2.903 724 377 034 119 589(5)	—
	2.903 724 377 034 15(28)	
1s2s	2.145 974 046 054 412(3)	2.175 229 378 236 791 300(8)
	2.145 974 046 054 28(11)	*2.175 229 378 236 791 0(3)*
1s3s	2.061 271 989 740 87(2)	2.068 689 067 472 454(6)
1s4s	2.033 586 716 88(17)	2.036 512 083 098 1(3)
1s5s	2.021 176 851 15(6)	2.022 618 872 30(1)
1s6s	2.014 563 097 4(6)	2.015 377 452 99(1)
1s7s	2.010 625 775 3(4)	2.011 129 919 51(1)
1s8s	2.008 093 619 1(5)	2.008 427 121 99(16)
1s9s	2.006 369 551 1(10)	2.006 601 516 45(21)
1s10s	2.005 142 987 4(27)	2.005 310 794 1(8)
1s11s	2.004 239 408(4)	2.004 310 794(4)
1s12s	2.003 554 611(7)	2.003 650 618(8)
1s13s	2.003 023 271(8)	2.003 098 445(16)
1s14s	2.002 602 732(10)	2.002 662 66(4)
1s15s	2.002 264 191(11)	2.002 312 67(8)
1s16s	2.001 987 2(3)	

3. Representation of the resonance parameters

As mentioned in the introduction the goal of this paper is twofold, firstly to provide numerical data of high quality for two-electron resonances over a wide range of energy, and secondly to examine the current understanding of two-electron resonances in terms of their classification by approximate quantum numbers (Herrick 1983, Lin 1986, Feagin and Briggs 1988) and in terms of the predicted propensity rules for autoionization (Rost and Briggs 1990, 1991). We will also comment on the role of classical orbits for the understanding of two-electron resonances in particular for high excitations (Ezra *et al* 1991, Müller *et al* 1992, Wintgen *et al* 1994).

However, for the presentation of the enormous data material in some ordered fashion we need a 'neutral' tool which does not anticipate the possible classification according to the aforementioned schemes. Our principal tool will be single- and multi-channel quantum defect theory. At high energies an ordering according to the quantum defects as we derive them from our data is not unique and we need an additional criterion to determine to which subseries the resonance should belong. In these cases we use the expectation value $\langle\cos\theta\rangle$ of the inter-electronic angle as a guideline.

3.1. Labelling and quantum numbers

The complex eigenvalues obtained by the method described above can be characterized by three indices, $E = E_{Nkn}$. The first index N denotes the principal quantum number of the electron in the remaining He^+ ion once the outer electron is ionized. For successively higher excitation of the outer electron with principal quantum number n the corresponding Rydberg series converge to the threshold $E_N = -Z^2/2N^2$ in the limit $n \to \infty$. There are N different Rydberg series of singlet states converging to each threshold because there are N different possibilities to couple the single particle angular momenta to $L = 0$. Note, however, that those single particle angular momenta are no longer good quantum numbers as in the independent-electron picture because of the strong electron–electron correlation.

Each of these Rydberg series converging to the same threshold is labelled by the index k which asymptotically ($n \to \infty$) determines the parabolic quantum numbers of the Stark–type state in which the inner electron resides (Rost and Briggs 1991). The index k, $k = -N+1, -N+3, \ldots, N-3, N-1$, is therefore related to the expectation value of $\cos\theta$, where θ is the angle between the two electron position vectors r_1 and r_2

$$\langle\cos\theta\rangle \underset{n\to\infty}{\longrightarrow} -\frac{k}{N}. \tag{11}$$

We see from (11) that for extremely high excitation $N \to \infty$ of the inner electron we get two collinear configurations with minimum angle $\langle\cos\theta\rangle \to (N-1)/N \approx +1$ which corresponds to a configuration with both electrons on the same side of the nucleus ($\theta \approx 0°$, the 'frozen planet states', Richter *et al* (1992)) and $\langle\cos\theta\rangle \to -(N-1)/N \approx -1$ where the electrons are localized on different sides of the nucleus ($\theta \approx 180°$, an 'asymmetric stretch', Rost *et al* (1991)). These two collinear configurations can be represented classically by characteristic periodic orbits which surprisingly are stable for the $\theta \approx 0°$ case and moderately unstable for the $\theta \approx 180°$ case (Ezra *et al* 1991, Richter and Wintgen 1991).

In what follows we use the nomenclature $(N,k)_n$ to identify a single state and (N,k) to specify a whole series. However, this classification is only unique in the limit $n \to \infty$ where perturbation theory can be applied and the He^+–electron interaction can be diagonalized in a stark basis of the He^+ ion (Gailitis and Damburg 1963). It has been a puzzle for a long time that the asymptotic ($n \to \infty$) classification holds also for states where both electrons are equally excited ($n \approx N$). This was first realized by Herrick in a group theoretical approach (Herrick 1983). His set of quantum numbers consists of $(\boldsymbol{N},\boldsymbol{K},\boldsymbol{T},\boldsymbol{n})$ where $(\boldsymbol{N},\boldsymbol{K},\boldsymbol{n})$ corresponds to our labels (N,k,n) and $\boldsymbol{T}$ is the projection of the total angular momentum on the inter-electronic axis (related to M' in our nomenclature, see (2)). Of course for $L = 0$ we have $\boldsymbol{T} = M' = 0$. To specify the character of the electron exchange symmetry (Pauli principle) one needs a fifth quantum number which is according to Lin (1986) commonly referred to as $\boldsymbol{A} = \pm 1$ (Herrick himself called it ν). In the case of $L = 0$ states $\boldsymbol{A} = +1$ corresponds to ^1S states and $\boldsymbol{A} = -1$ to ^3S states. For the relation to other classification schemes see e.g. Rost and Briggs (1991).

3.2. *Quantum defects*

To the extent to which the separation of the resonances into series holds, the (complex) energies can be conveniently parameterized by the ansatz

$$E_{Nkn} = -\frac{Z^2}{2N^2} - \frac{(Z-1)^2}{2\nu_{kn}^2} = -E_N - \frac{(Z-1)^2}{2(n-\mu_{kn})^2} \tag{12}$$

where ν_{kn} is an effective quantum number for the outer electron and μ_{kn} is its quantum defect. According to this ansatz the total energy of the system consists of the energy of the inner (outer) electron in the field of the unshielded (shielded) nucleus only; all discrepancies from this simple picture are collectively described by the μ_{kn}. Note that since the E_{Nkn} are complex for doubly excited states, ν_{kn} and μ_{kn} are also complex. The real part of the quantum defect determines the energy shift (in units of the nodal number n) whereas the imaginary part gives the rescaled width $\Gamma\nu_{kn}^3$.

The discrete points μ_{kn} lie on a continuous curve $\mu(E)$. For unperturbed Rydberg series the quantum defect is a slowly varying function of the energy (Seaton 1983, Wintgen and Friedrich 1987). Already for moderate excitation of the inner electron, however, Rydberg series converging to different thresholds of the He^+ ion begin to overlap leading to a perturbation of the Rydberg series (Bürgers and Wintgen 1994). This can be described within a three-channel quantum defect theory (3QDT) where the first channel contains one state (the so called perturber), the second one the unperturbed Rydberg series under consideration, and the third channel is open (Wintgen and Friedrich 1987). The real and imaginary part of the quantum defect is then parameterized as follows:

$$\mathrm{Re}\,\mu(E) = \bar{\mu}(E) - \frac{1}{\pi}\arctan\left(\frac{1}{\epsilon}\right) \tag{13}$$

$$\mathrm{Im}\,\mu(E) = \bar{\gamma}(E) + \gamma_0\frac{(q+\epsilon)^2}{1+\epsilon^2}\,, \tag{14}$$

where $\epsilon = (E - E_R)/(\Gamma/2)$ measures the energy with respect to the location E_R of the perturber in units of its half width $\Gamma/2$. The quantities $\bar{\mu}(E)$ and $\bar{\gamma}(E)$ are slowly varying backgrounds of the quantum defect (real part) and the reduced width (imaginary part), γ_0 is the amplitude of the Fano–type modulation in (14) (Fano 1961, Wintgen and Friedrich 1987).

The perturbing state itself does not appear as an isolated state but becomes an additional member of the perturbed Rydberg series. All the states in a confined region in the vicinity of the perturber (and also the perturber itself) are shifted due to the interaction between the corresponding channels. Far from the perturbed zone the series remains unperturbed, but since one state has been added the numbering has changed and the quantum defect increases by unity. The location and width of such a perturber can be determined by fitting (13) and (14) to the resonance data.

This picture also holds for more than one perturber resulting in several arctan-shaped 'jumps' provided the perturbers do not interfere. If they do the picture becomes more complicated since the interaction of the perturbers significantly changes both the location and the width of the pseudoresonant jumps (Friedrich 1991).

Since the pseudoresonant perturber is not a true resonant state it does not appear in a converged numerical calculation as a single (complex) eigenvalue. This remains true even for non-converged calculations as long as, in the truncated basis, the dense Rydberg states forming the pseudocontinuum are well represented. However, if one deliberately chooses the basis parameters a, c, β so that the Rydberg states are *badly* represented, the

pseudocontinuum no longer 'exists' and the perturber itself occurs as an isolated state. These states are only fairly well converged since enlarging the basis size also improves the representation of the pseudocontinuum. The situation becomes better the closer the perturber is to the corresponding ionization threshold. Hence by using a 'detuned' basis we can calculate directly the location and width of the perturbers and compare them to those values obtained by a 3QDT fit.

4. The spectrum of the He atom

4.1. Overview

We have calculated doubly excited states for the helium atom for both singlet and triplet symmetry up to $N = 10$. Our calculations have been performed for infinite nuclear mass ($M \rightarrow \infty$). A non-perturbative inclusion of the finite nuclear mass, however, does not lead to any difficulties and is already implemented in our computer code.

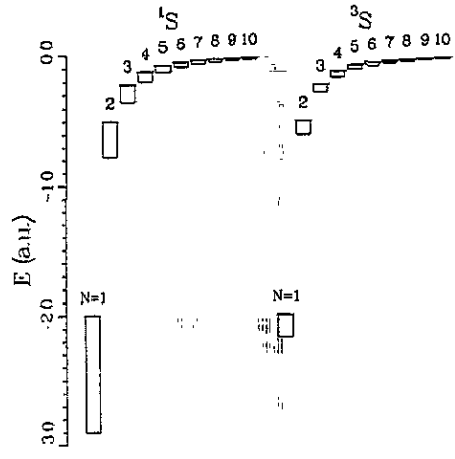

Figure 1. Sketch of the helium doubly excited spectrum for $L = 0$. We only show the lowest state for each threshold up to $N = 10$. The various states lie in the range indicated by the rectangles. Both the singlet and the triplet system are shown.

Figure 1 schematically shows the spectrum of the He atom for both the singlet (left) and the triplet (right) symmetry. Only the lowest state and the thresholds are shown, indicating the energy range of the (resonant) states. For small N ($N < 4$ in the singlet case and $N < 6$ in the triplet case) the Rydberg series converging to different thresholds are energetically well separated and the spectrum is rather simple. Hence the quantum defects of the respective series should be slowly varying functions of the energy.

For larger N the Rydberg series converging to different thresholds begin to overlap energetically and we find that the Rydberg series are perturbed. As already shown in Bürgers and Wintgen (1994) the perturbation scheme for moderately excited series follows the propensity rules derived by Rost and Briggs (1990, 1991) in a molecular orbital approach. For very highly excited sates and $k \approx 0$, that is far from a collinear configuration, it is no longer clear whether a k index can still be assigned and the propensity rules break down.

In the following we will present our results in detail. For the sake of clarity we will focus on the series with singlet symmetry. In general, singlet and triplet spectra show

the same features. However, since triplet manifolds are energetically more separated than singlet manifolds (see figure 1) the phenomena of perturbed Rydberg series start for higher N in the triplet case.

4.2. *The unperturbed Rydberg series ($N = 2, 3$)*

Table 2. Energies for the $(2, k)$ Rydberg series (in au).

state			^{1}S		^{3}S	
N	k	n	$-\mathrm{Re}\,E$	$-\mathrm{Im}\,E$	$-\mathrm{Re}\,E$	$-\mathrm{Im}\,E$
2	1	2	0.777 867 636	0.002 270 653	—	—
		3	0.589 894 682	0.000 681 239	0.602 577 505	0.000 003 325
		4	0.544 881 618	0.000 246 030	0.548 840 858	0.000 001 547
		5	0.526 686 857	0.000 109 335	0.528 413 972	0.000 000 771
		6	0.517 641 112	0.000 056 795	0.518 546 375	0.000 000 428
		7	0.512 513 488	0.000 032 992	0.513 046 496	0.000 000 260
		8	0.509 332 686	0.000 020 795	0.509 672 798	0.000 000 169
		9	0.507 225 835	0.000 013 936	0.507 456 056	0.000 000 116
		10	0.505 759 104	0.000 009 790	0.505 922 151	0.000 000 082
	−1	2	0.621 927 254	0.000 107 818	—	—
		3	0.548 085 535	0.000 037 392	0.559 746 626	0.000 000 130
		4	0.527 716 640	0.000 023 101	0.532 505 349	0.000 000 072
		5	0.518 104 252	0.000 014 894	0.520 549 199	0.000 000 041
		6	0.512 763 242	0.000 009 970	0.514 180 356	0.000 000 025
		7	0.509 483 569	0.000 006 918	0.510 378 174	0.000 000 016
		8	0.507 324 340	0.000 004 959	0.507 925 149	0.000 000 011
		9	0.505 827 143	0.000 003 657	0.506 250 079	0.000 000 008
		10	0.504 746 388	0.000 002 766	0.505 055 341	0.000 000 006

The data calculated for the $(2, k)$ and $(3, k)$ series are given in table 2 and table 3, respectively. As can be seen, the triplet states lie a little below the corresponding singlets. This is clear because the node in the triplet wavefunction at $r_1 = r_2 = 0$ reduces the electron–electron repulsion. As a consequence, the widths of the triplet states are about two orders of magnitude smaller than those of the corresponding singlet states. The character of the wave function on the Wannier saddle $r_1 = r_2$ is essential for the decay mechanism (Rost and Briggs 1990) and for the separation of different Rydberg series labeled by k (see above).

In principle we could extend our calculation for these states both to obtain more accuracy and for higher n values. However, at this stage relativistic effects should become significant which have not been included yet. Moreover, high n states can be calculated with almost the same accuracy by simply fitting the quantum defects as a function of n.

4.3. *Simply perturbed Rydberg series ($N = 4, 5$): confirmation of the propensity rules*

We now come to the region where the Rydberg series converging to different thresholds of the He^+ ion begin to overlap energetically. This has a drastic effect on the complex resonance energies which is obvious in the quantum defect μ_{kn}.

Figure 2 shows the real part of the quantum defect for the four Rydberg series converging to the $N = 4$ threshold. The quantum defects of the three energetically higher Rydberg series ($k = 1, -1, -3$) are smooth functions of the energy. The quantum defect for the

Table 3. Energies for the $(3, k)$ Rydberg series (in au).

state			^1S		^3S	
N	k	n	$-\mathrm{Re}\,E$	$-\mathrm{Im}\,E$	$-\mathrm{Re}\,E$	$-\mathrm{Im}\,E$
3	2	3	0.353 538 536	0.001 504 906	—	—
		4	0.281 072 703	0.000 750 733	0.287 277 138	0.000 014 914
		5	0.255 972 114	0.000 350 036	0.258 133 976	0.000 009 748
		6	0.243 824 049	0.000 179 910	0.244 807 489	0.000 005 801
		7	0.237 147 099	0.000 102 160	0.237 672 213	0.000 003 578
		8	0.233 121 363	0.000 062 881	0.233 433 327	0.000 002 322
		9	0.230 519 146	0.000 041 369	0.230 719 088	0.000 001 578
		10	0.228 744 234	0.000 028 755	0.228 880 000	0.000 001 117
		11	0.227 481 269	0.000 020 794	0.227 577 8	0.000 000 8
		12	0.226 551 500	0.000 015 492		
	0	3	0.317 457 836	0.003 329 920	—	—
		4	0.263 388 312	0.001 209 354	0.270 283 614	0.000 023 308
		5	0.246 634 603	0.000 565 481	0.249 000 418	0.000 006 848
		6	0.238 524 104	0.000 318 437	0.239 696 887	0.000 004 600
		7	0.233 898 812	0.000 196 262	0.234 569 038	0.000 003 061
		8	0.231 001 524	0.000 129 185	0.231 421 646	0.000 002 100
		9	0.229 064 586	0.000 089 418	0.229 345 782	0.000 001 491
		10	0.227 705 232	0.000 064 398	0.227 902 914	0.000 001 091
		11	0.226 714 42	0.000 047 89	0.226 859	0.000 001
	−2	3	0.257 371 610	0.000 010 564	—	—
		4	0.244 324 739	0.000 021 400	0.249 964 616	0.000 006 789
		5	0.237 311 202	0.000 017 021	0.240 314 494	0.000 003 490
		6	0.233 173 689	0.000 012 347	0.234 969 582	0.000 002 042
		7	0.230 531 347	0.000 008 810	0.231 692 116	0.000 001 300
		8	0.228 741 812	0.000 006 247	0.229 535 701	0.000 000 880
		9	0.227 473 958	0.000 004 545	0.228 040 873	0.000 000 623
		10	0.226 542 99	0.000 003 42	0.226 962	0.000 001

$(N, k) = (4, 3)$ Rydberg series, however, increases rather suddenly by unity around 0.04 au below the $N = 4$ threshold (which is located at -0.125 au). This pseudoresonant jump is caused by the lowest doubly excited state of the $N = 5$ Rydberg series, namely the $(N, k)_n = (5, 4)_5$ state, which does not appear as an individual state but compresses the dense spectrum of the (4, 3) Rydberg series (Bürgers and Wintgen 1994).

In figure 3 both the real and imaginary part of the quantum defect of the (4, 3) Rydberg series are shown. The solid lines are fits to (13) and (14), respectively, where $\bar{\mu}(E)$ is fitted by a polynomial of degree 2 and $\bar{\gamma}(E)$ by a polynomial of degree 1. The data are obviously in excellent agreement with the predictions of the 3QDT. This indicates that the $(5, 4)_5$ state mixes with the $(N, k) = (4, 3)$ Rydberg series and not with the (4, 1), (4, −1) or (4, −3) series.

Furthermore, the lifetime of the states energetically close to the pseudoresonant jump is drastically enhanced. Although the width of the states affected does not vanish the fitted Fano profile has an approximate zero between the $(4, 3)_{11}$ and $(4, 3)_{12}$ states (Bürgers and Wintgen 1994). Such a behaviour can only be expected if there is effectively only one open channel for the perturbed series to decay to, though in principle there should be six. The data hence confirm the propensity rules for the non-radiative decay (Rost and Briggs 1990, 1991)

$$\Delta N = -1 \qquad \Delta k = -1. \tag{15}$$

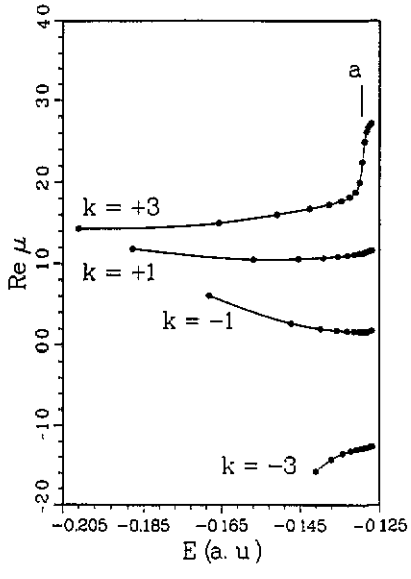

Figure 2. Quantum defect (real part) for the $(4, k)$ Rydberg series (singlet symmetry). The location of the perturber is marked by a small solid line (a).

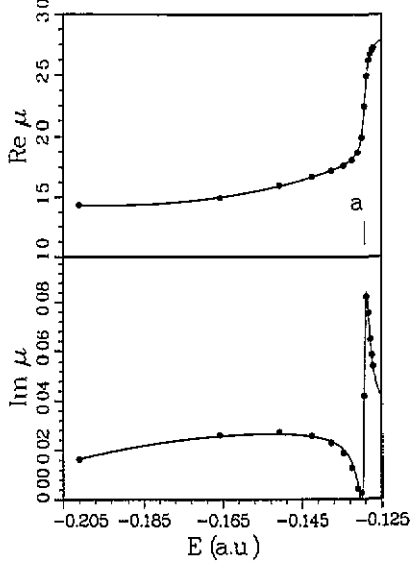

Figure 3. Real and imaginary part of the quantum defect of the (4, 3) Rydberg series (singlet symmetry). The solid line here represents a 3QDT fit to our data (see text). The location of the perturber is marked by the small solid line (a).

Another confirmation of the propensity rules (15) is provided by the comparison of the location E_R and width Γ of the perturber obtained by the fit of the 3QDT functions to the complex eigenvalue obtained by the 'exact' calculations. Whereas the fit to the 3QDT gives the partial width of the perturber for the decay into the Rydberg series, the complex rotation calculation gives its total decay width for non–radiative decay. Both widths are

Table 4. Energies for the $(4, k)$ Rydberg series (in au).

state			^1S		^3S	
N	k	n	$-\mathrm{Re}\,E$	$-\mathrm{Im}\,E$	$-\mathrm{Re}\,E$	$-\mathrm{Im}\,E$
4	3	4	0.200 989 572	0.000 969 178	—	—
		5	0.165 734 021	0.000 605 047	0.169 306 635	0.000 021 006
		6	0.150 824 382	0.000 320 293	0.152 122 029	0.000 016 799
		7	0.142 602 474	0.000 169 806	0.143 175 987	0.000 011 381
		8	0.137 685 346	0.000 092 512	0.137 961 324	0.000 007 642
		9	0.134 551 108	0.000 049 711	0.134 679 533	0.000 005 256
		10	0.132 451 935	0.000 023 393	0.132 490 651	0.000 003 725
		11	0.130 999 124	0.000 005 799	0.130 962 374	0.000 002 717
		12	0.129 993 447	0.000 002 704	0.129 855 236	0.000 002 035
		13	0.129 322 969	0.000 033 799	0.129 028 519	0.000 001 559
		14	0.128 776 594	0.000 054 043	0.128 395 405	0.000 001 219
		15	0.128 262 189	0.000 039 756	0.127 900 092	0.000 000 970
		16	0.127 815 73	0.000 027 43	0.127 505 44	0.000 000 79
		17	0.127 446 1	0.000 020 0	0.127 186 0	0.000 000 6
		18	0.127 141 5	0.000 015 2		
	1	4	0.187 834 626	0.002 458 380	—	—
		5	0.156 904 051	0.001 377 256	0.161 480 663	0.000 051 980
		6	0.145 397 764	0.000 808 943	0.147 168 813	0.000 037 116
		7	0.139 189 490	0.000 475 268	0.139 998 046	0.000 020 176
		8	0.135 437 398	0.000 289 889	0.135 857 413	0.000 015 013
		9	0.132 996 200	0.000 183 914	0.133 230 435	0.000 010 505
		10	0.131 319 807	0.000 120 624	0.131 456 986	0.000 007 547
		11	0.130 120 051	0.000 080 068	0.130 202 295	0.000 005 577
		12	0.129 224 756	0.000 057 660	0.129 281 536	0.000 004 228
		13	0.128 551 852	0.000 041 001	0.128 585 657	0.000 003 276
		14	0.128 025 335	0.000 027 559	0.128 046 838	0.000 002 588
		15	0.127 605 478	0.000 019 886	0.127 621 073	0.000 002 078
		16	0.127 267 459	0.000 015 312	0.127 278 774	0.000 001 694
		17	0.126 991 2	0.000 012 3	0.126 999 3	0.000 001 4

the same within the accuracy of the fit: the fitted value is $E = -0.129\,24 - \mathrm{i}\,0.000\,63$, the numerically converged value is $E = -0.129\,43 - \mathrm{i}\,0.000\,69$. From this we conclude that the decay is effectively only according to the propensity rules (15).

The energies of the $(4, k)$ series are listed in table 4 for both symmetries. Note that the $(4, 3)$ triplet series is still unperturbed. Also, the width for the series with the minimum $k = -(N - 1) = -3$ is in both cases considerably smaller than for the other series belonging to the same symmetry. This is a general trend (see also the $(3, -2)$ series in table 3) and can also be understood in terms of the propensity rules: The favoured decay channel $(N - 1, k - 1)$ does not exist for these states which must hence decay with a smaller rate to less favourite channels. This effect will become even more pronounced with increasing N. Note that these states are just the 'frozen planet' states described classically and semiclassically in (Richter and Wintgen 1991, Richter *et al* 1992).

Figure 4 shows the real part of the quantum defect of the Rydberg series converging to the $N = 5$ threshold of the He^+ ion. The lowest state of the $(5, 4)$ series does not really exist as an isolated state. The quantum defect of the perturber is shown instead (indicated by the open symbol lying below the $N = 4$ threshold which is indicated by the dotted line). In figure 4 we see already three pseudoresonant jumps in the lower lying series with $k = 4, 2, 0$

Table 4. Continued.

state			^1S		^3S	
N	k	n	$-\mathrm{Re}\,E$	$-\mathrm{Im}\,E$	$-\mathrm{Re}\,E$	$-\mathrm{Im}\,E$
4	−1	4	0.168 261 328	0.001 086 186	—	—
		5	0.147 266 965	0.000 416 449	0.151 176 420	0.000 022 408
		6	0.139 840 342	0.000 239 815	0.141 691 356	0.000 014 696
		7	0.135 728 512	0.000 160 253	0.136 787 119	0.000 009 622
		8	0.133 141 846	0.000 111 361	0.133 811 711	0.000 006 493
		9	0.131 396 547	0.000 080 331	0.131 849 211	0.000 004 540
		10	0.130 160 039	0.000 059 877	0.130 480 976	0.000 003 283
		11	0.129 251 251	0.000 046 022	0.129 487 225	0.000 002 444
		12	0.128 562 811	0.000 036 493	0.128 742 039	0.000 001 867
		13	0.128 029 833	0.000 031 311	0.128 168 616	0.000 001 457
		14	0.127 610 012	0.000 025 737	0.127 717 807	0.000 001 158
		15	0.127 271 404	0.000 020 669	0.127 356 918	0.000 000 935
		16	0.126 994 4	0.000 016 6	0.127 063 50	0.000 000 77
	−3	4	0.141 064 156	0.000 011 739	—	—
		5	0.137 088 229	0.000 002 490	0.140 088 484	0.000 004 409
		6	0.134 228 598	0.000 002 711	0.135 975 513	0.000 001 752
		7	0.132 212 660	0.000 003 293	0.133 329 246	0.000 001 340
		8	0.130 772 717	0.000 003 289	0.131 533 731	0.000 001 087
		9	0.129 717 890	0.000 002 986	0.130 261 370	0.000 000 886
		10	0.128 925 097	0.000 002 597	0.129 327 395	0.000 000 724
		11	0.128 315 304	0.000 002 218	0.128 621 731	0.000 000 593
		12	0.127 836 684	0.000 001 881	0.128 075 620	0.000 000 489
		13	0.127 454 353	0.000 001 595	0.127 644 351	0.000 000 407
		14	0.127 144 218	0.000 001 356	0.127 297 839	0.000 000 341
		15	0.126 889 26	0.000 001 18	0.127 015 24	0.000 000 29

where the jump in the $(N, k) = (5, 0)$ series takes place very close to the $N = 6$ threshold and is not completely visible in figure 4. The jumps stem from the three different perturbers of the $N = 6$ series with $k = 5, 3, 1$, respectively. Although each perturber (indicated as a vertical line in figure 4) is energetically close to states from different series $(5, k)$ the perturber $(6, k)_6$ influences *only* states from the $(5, k-1)_n$ series. Hence the perturbation scheme is regular obeying the propensity rules (15) for autoionizing decay. Here again the location and width of the several perturbers can be obtained either by fitting (13) and (14) to the data or by a direct calculation. Again, the results agree within the accuracy.

An adiabatic description for the three-body dynamics, in particular the molecular orbital (MO), allows for an alternative interpretation of the propensity rules (15). The major coupling scheme between adiabatic MO channels comes from avoided crossings which are caused by the saddle in the potential for fixed adiabatic separation of the electrons (Rost and Briggs 1991). The MO Potentials are characterized uniquely by the spheroidal quantum numbers (n_λ, n_μ, m). On the other hand the coupling mechanism through the saddle of the potential is not restricted to a MO adiabatic representation. It can also be seen from the widely used hyperspherical adiabatic representation for which the prolate spheroidal quantum numbers do not apply. If we denote an adiabatic channel more generally by Herrick's quantum numbers as $|NKT\rangle$ † (Herrick 1983), then (15) is an expression for the dominant coupling

† The relation between Herrick's and the MO quantum numbers is: $T = |m|$, $K = [n_\mu/2] - n_\lambda$, $N = n_\lambda + [n_\mu/2] + |m| + 1$ where $[x]$ denotes the integer value of x.

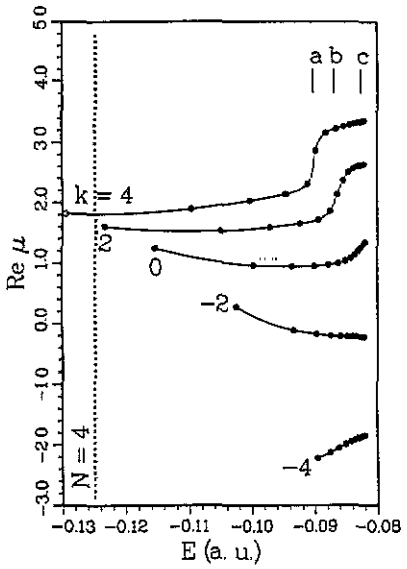

Figure 4. Quantum defect (real part) for the $(5, k)$ Rydberg series (singlet symmetry). Note that the lowest state of the $(5, 4)$ series is the perturber of the $(4, 3)$ series, it is therefore marked by an open circle. The locations of the perturbers of the $(5, k)$ series are marked: a = $(6, 5)_6$, b = $(6, 3)_6$, c = $(6, 1)_6$.

between adiabatic channels and should read

$$\Delta N = -1 \qquad \Delta K = -1 . \tag{16}$$

Hence, the existence of the propensity rule according to (15) is a strong indication that the Rydberg series shown in figures 2 and 4 can each be represented by a *single* adiabatic channel $|NkM'\rangle = |NKT\rangle$. A violation of the propensity rules (15) indicates from this perspective that the respective Rydberg series is no longer a pure adiabatic $|NKT\rangle$ channel but a mixture of those: $|NkM'\rangle = \sum_i a_i |N_i K_i T_i\rangle$. For S states, M' and the T_i are zero. We will drop them in the following and write (N, k) for $|N\,k\,M' = 0\rangle$.

4.4. Few channel interferences (N=6, 7)

Figure 5 shows the real part of the quantum defect for the Rydberg series converging to the $N = 6$ threshold of the He^+ ion (singlet symmetry). The lower lying $(6, 5)$ and $(6, 3)$ series are already twice perturbed, although only the beginning of the second perturbation of the $(6, 3)$ series is slightly visible in our data. The corresponding perturbers can be labelled as $(7, 6)_7$, $(7, 6)_8$, $(7, 4)_7$, and $(7, 4)_8$ respectively, where the last one can only be determined by a direct calculation in a 'detuned' basis (see section 3.2). The other three can also be fitted; the results again agree within their accuracy. On the other hand the two energetically highest series $(6, -3)$ and $(6, -5)$ display the normal behaviour of unperturbed Rydberg series. So far, the perturbation pattern is consistent with the propensity rules (15) and hence with pure adiabatic channels.

However, in the $(6, 1)$ and $(6, -1)$ series a new behaviour occurs. The quantum defect in the $(6, 1)$ series increases by more than unity (by 1.2 roughly), whereas the quantum defect in the $(6, -1)$ series increases by less than one (about 0.8), giving a total 'jump' of two. A closer inspection of the $(6, 1)$ series shows that the jump here actually consists

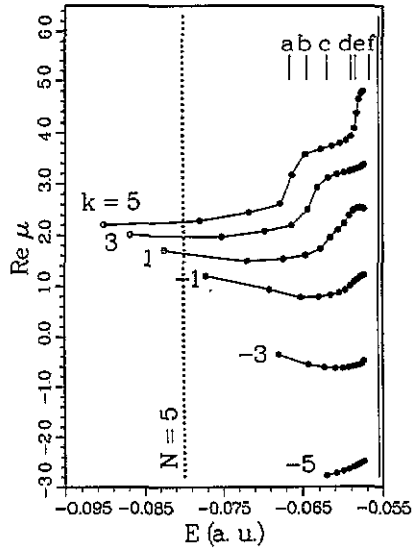

Figure 5. As in figure 5, but for the $(6, k)$ Rydberg series. The perturbers are: a = $(7, 6)_7$, b = $(7, 4)_7$, c = $(7, 2)_7$, d = $(7, 0)_7$, e = $(7, 6)_8$, f = $(7, 4)_8$.

of two parts, a first one by unity and a smaller one. This first jump is located at the energy of the $(7, 2)_7$ perturber. The second 'jump' coincides energetically with the location of the $(7, 0)_7$ perturber that, according to (15), should only couple to the $(6, -1)$ series. Obviously, the $(7, 0)_7$ perturber affects the $(6, 1)$ and the $(6, -1)$ Rydberg series, *violating the propensity rules* (15).

This behaviour indicates in the context of our discussion in section 4.3 that the index k as a quantum number is no longer 'pure' for channels with $k \approx 0$. Apparently the pure $K = +1$ and $K = -1$ channels are mixed resulting in the observed $(6, 1)$ and $(6, -1)$ Rydberg series. Through this admixture the $(7, 0)_7$ perturber which according to the propensity rules (16) should couple to the $K = -1$ adiabatic channel affects both, the $(6, 1)$ and $(6, -1)$ series. Hence, the perturbation can be viewed as a sensitive tool probing the components of effective Rydberg series in terms of their pure K components.

Note that the perturbation pattern caused by the $(7, 0)_7$ perturber can still be described by a quantum defect theory, adding another Rydberg series and continuum to which the perturber is coupled. A model calculation of the corresponding 5QDT reveals a similar behaviour as the real atom if the coupling of the perturber to the two Rydberg series is of about the same magnitude.

We do not discuss in detail the Rydberg series $(7, k)$ which show qualitatively a similar behaviour as the $(6, k)$ series.

4.5. Breakdown of the propensity rules ($N \geqslant 8$)

Figure 6 shows the real part of the quantum defect belonging to the $(8, k)$ Rydberg series of singlet symmetry. The $N = 7$ threshold is denoted by a dotted line. The open symbols below that threshold represent the perturbers.

The two lowest lying series ($(8, 7)$ and $(8, 5)$) are again perturbed Rydberg series that can be described by means of a FQDT. Note that the fourth perturbation of the $(8, 7)$ series

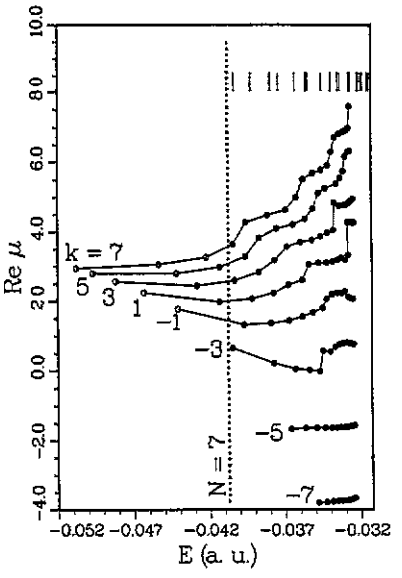

Figure 6. As in figure 5, but for the $(8, k)$ Rydberg series.

is very narrow. The reason is that the $(9, 8)$ series perturbing it is itself already perturbed by the lowest state of the $(10, 9)$ series, namely $(10, 9)_{10}$. The propensity rules (15) are fulfilled for these series which hence can be regarded as pure K series. This is also true for the two energetically highest series $(8, -5)$ and $(8, -7)$ which display the behaviour of unperturbed Rydberg series.

The series in between $(k = 3, \ldots, -3)$ show rather irregular behaviour. Obviously these are no pure K channels. Hence, the calculated $(8, k)$ Rydberg series as shown in figure 6 are mixtures of those pure K channels as discussed above. For these series also the first states occur whose reduced width $(\mathrm{Im}\,\mu)$ is larger than one, which means that their width is larger than their mutual spacing. These are the $(8, 1)_{21}$ state $(\mathrm{Im}\,\mu = 1.507\,51)$ and the $(8, -1)_{14}$ state $(\mathrm{Im}\,\mu = 1.278\,83)$.

The behaviour of the $(9, k)$ and $(10, k)$ series (shown in figure 7) is similar. For the energetically lowest series (larger k) we find Rydberg series perturbed according to (15), which can be described by an FQDT. For the energetically highest series (lower k) we find, as before, the typical behaviour of unperturbed series.

In between, however, we have the region where the series obviously consist of mixtures of pure K channels resulting in a rather complicated perturbation scheme. Here a FQDT analysis from our data is no longer possible. This is demonstrated by looking at the expectation value of the cosine of the inter-electronic angle, $\langle\cos\theta\rangle$. It is connected with the quantum number K through $\langle\cos\theta\rangle \to -K/N$ as $n \to \infty$ (see also (11)). We have plotted $\langle\cos\theta\rangle$ against ν_{kn} for the $(10, k)$ series in figure 8. Obviously the pattern is rather irregular, which also stresses that the actual states consist of complicated mixtures in terms of the pure K channels. The region for which this admixtures occur is located near $k \approx 0$ and becomes the wider, the larger N. This can be understood in terms of the adiabatic approach (Rost and Briggs 1991) since the separation of the adiabatic potentials for different k goes with k/N leading to a greater possibility for the channels to couple. Assigning a k index to the calculated resonances in this region obviously becomes rather arbitrary. Hence it is problematic to speak of k as a quantum number for these states. Note that the $k \approx 0$

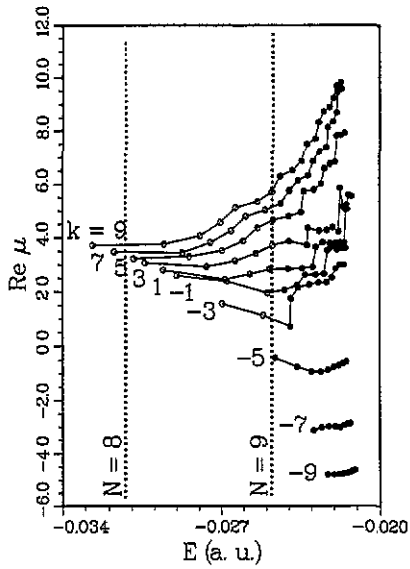

Figure 7. As in figure 5, but for the $(10, k)$ Rydberg series.

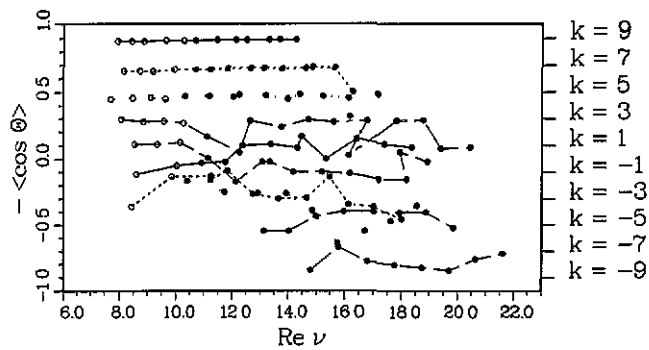

Figure 8. Expectation values for $\cos\theta$ versus the effective quantum number $\mathrm{Re}\,\nu$ for the $(10, k)$ Rydberg series (singlet symmetry). The lines connect states which belong to the same k series. Here the k index is assigned by the requirement that the quantum defect should not cross. An assignment of k according to equation (11) is not possible since the asymptotic limit $n \gg N$ of the series has not been reached. It illustrates that the affected states are admixtures of pure K states even for n as high as $2N$.

states are just those states whose configuration is far from being collinear and hence do not approach one of the classical limits discussed above. This might explain why they do not behave in a regular fashion for increasing N.

4.6. Triplet states

In general the spectrum for the triplet states ($A = -1$) looks quite similar to that of singlet symmetry ($A = +1$). The qualitative difference is the additional node on the saddle ($r_1 = r_2$) for triplet symmetry. This leads to wider avoided crossings in the corresponding adiabatic potentials than in the singlet case and hence the probabilities for auto-ionization and for K mixing are reduced (Rost and Briggs 1991). Furthermore, the different ($A = -1$)

adiabatic channels start to interact at higher quantum numbers than the ($A = +1$) channels. As a consequence the first perturbed triplet series are the (6, 5), (6, 3), and (6, 1) series while the first perturbed singlet series occurs with the (4, 3) series already in the $N = 4$ manifold.

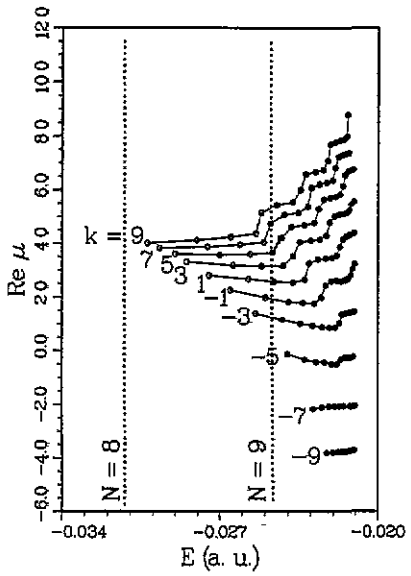

Figure 9. Quantum defect (real part) for the $(10, k)$ Rydberg series. Open symbols mark the perturbers of the underlying series.

Figure 9 shows the real part of the quantum defect for the $(10, k)$ triplet Rydberg series. Here, violations of the propensity rules (15) occur for the $(10, -3)$ and $(10, -5)$ Rydberg series indicating that these are also mixtures of pure K adiabatic channels. However, the pattern looks much simpler than for the $(10, k)$ singlet series. This confirms that the mixing of K channels for states with triplet symmetry is much weaker than in the singlet case.

4.7. Propensity rules versus selection rules

The *propensity* rules (15) are not *selection* rules. This can be demonstrated by a closer inspection of our data even for the case where the propensity rules are fulfilled to a very good approximation, namely for the very lowest case of a perturbed Rydberg series.

In figure 10 we again show the quantum defect of the singlet $(4, k)$ Rydberg series, but now we subtract multiples of unity from the quantum defect to display possible degeneracies. The region where the quantum defects cross is enlarged in the upper right part of figure 10. The (4, 1) series shows little deviation from the regular behaviour close to the location of the perturber of the (4, 3) series. Though this perturbation is very weak it indicates a small coupling of the $(5, 4)_5$ perturber to the (4, 1) series. This is, however, a marginal effect. The non-radiant decay is still mainly according to the propensity rules (15).

5. Summary and Conclusion

To sum up we have calculated more than thousand doubly excited states for the He atom for both singlet and triplet symmetry of the wavefunction using the full non-relativistic

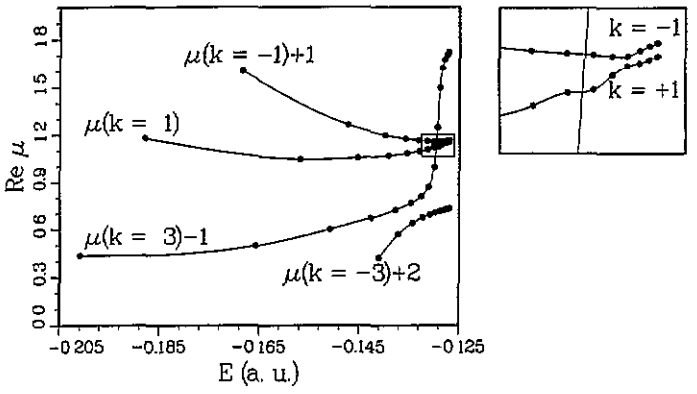

Figure 10. Quantum defects of the $(4, k)$ Rydberg series modulo 1 (see text). The upper right figure is an enlargement of the region marked by the rectangle.

Hamiltonian.

We have used the complex rotation technique to calculate resonance energies and widths of these states in an almost complete basis set of Sturmian type functions using perimetric coordinates as introduced by Coolidge and James (1937).

Our highly accurate data for the spectrum of helium confirm the known propensity rules (15) generally for moderate excitation. For very high excitations of the inner electron, however, the propensity rules are only valid for near-to-collinear configurations (minimum and maximum k). For series with maximum k values the spectrum can be described by means of a few-channel quantum defect theory (FQDT). This is the region where a semiclassical description using periodic orbit theory and cycle expansions (Richter *et al* 1992, Wintgen *et al* 1994) or adiabatic quantum ansätze (Rost and Briggs 1990, 1991, Sadeghpour 1991) are also valid.

For minimum k, the regular behaviour of unperturbed Rydberg series is observed. In this region a semiclassical EBK quantization (Richter and Wintgen 1991) is also possible.

For very hhighly doubly excited states far from a collinear configuration (k close to 0), the situation becomes much more complicated. The spectrum can no longer be described by a simple FQDT and the index k no longer has the meaning of a quantum number. Note that this region far from a collinear configuration is also inaccessible for both the semiclassical and the adiabatic approaches.

However, in the transition region of still identifiable Rydberg series we have shown how one can determine the pure adiabatic K-components of a perturbed series by linking the perturber states with the help of (16) to the K-components of these states.

Acknowledgments

We would like to thank John Briggs, Klaus Richter, and Gregor Tanner for many fruitful discussions. This work was supported by the Deutsche Forschungsgemeinschaft in the SFB 276 located in Freiburg.

Appendix 1. Transformation to perimetric coordinates

The transformation of the Hamiltonian (1) into perimetric coordinates (4) is done in two steps. In a first step the cartesian coordinates are transformed into the three distances r_1,

r_2, and r_{12} (Hylleraas 1929) and the three Euler angles ψ, θ, ϕ. Neither the kinetic energy nor the potentials depend on the angles, so they only contribute to the volume element by a factor of 8π. The three distances r_1, r_2, and r_{12} are then in a second step transformed to the perimetric coordinates, giving the Hamiltonian in the form (4). The $P_{ij}^{(3)}$ are (for $M \to \infty$):

$$\begin{aligned}
P_{xx}^{(3)} &= 2(x^2y + xy^2 + x^2z + xz^2) \\
P_{yy}^{(3)} &= 2(2x^2y + 2xy^2 + y^2z + yz^2 + 2xyz) \\
P_{zz}^{(3)} &= 2(2x^2z + 2xz^2 + y^2z + yz^2 + 2xyz) \\
P_{xy}^{(3)} &= P_{yx}^{(3)} = 2xy(x + y) \\
P_{xz}^{(3)} &= P_{zx}^{(3)} = 2xz(x + z) \\
P_{yz}^{(3)} &= P_{zy}^{(3)} = 0 .
\end{aligned}$$

References

Bathia A K and Temkin A 1975 *Phys. Rev.* A **11** 2018
——1984 *Phys. Rev.* A **29** 1895
Breit G 1930 *Phys. Rev.* **35** 569
Buchleitner A, Grémaud B, and Delande D 1994 *J. Phys. B: At. Mol. Opt. Phys.* **27** 2663
Bürgers A and Wintgen D 1994 *J. Phys. B: At. Mol. Opt. Phys.* **27** L131
Coolidge A S and James H M 1937 *Phys. Rev.* **51** 855
Delande D, Bommier A, and Gay J C 1991 *Phys. Rev. Lett.* **66** 141
Domke M, Remmers G and Kaindl G 1992 *Phys. Rev. Lett.* **69** 1171
Domke M, Schulz K, Remmers G, Gutiérrez A, Kaindl G and Wintgen D 1995 *Phys. Rev. Lett.* (submitted)
Domke M, Xue C, Puschmann A, Mandel T, Hudson E, Shirley D A, Kaindl G, Greene C H, Sadeghpour H R, and Petersen H 1991 *Phys. Rev. Lett.* **66** 1306
Drake G W F 1988 *Nucl. Instrum. Methods Phys. Res.* B **31** 7
Ezra G S, Richter K, Tanner G, and Wintgen D 1991 *J. Phys. B: At. Mol. Opt. Phys.* **24** L413
Fano U 1961 *Phys. Rev.* **124** 1866
Feagin J M and Briggs J S 1988 *Phys. Rev.* A **37** 4599
Friedrich H 1991 *Theoretical Atomic Physics* (New York: Springer) ch. 3
Froese-Fischer C and Indrees M 1990 *J. Phys. B: At. Mol. Opt. Phys.* **23** 679
Gailitis M and Damburg R 1963 *Proc. Phys. Soc. London* **82** 192
Herrick D 1983 *Adv. Chem Phys.* **52** 1
Ho Y K 1979 *J. Phys. B: At. Mol. Phys.* **12** 387
——1980 *Phys. Rev. Lett.* **79A** 44
——1981 *Phys. Rev.* A **23** 2137
——1983 *Phys. Rep.* **99** 1
——1986 *Phys. Rev.* A **34** 4402
Lin C D 1986 *Adv. At. Mol. Phys.* **22** 77
Lindroth E 1994 *Phys. Rev.* A **49** 4473
Madden R P and Codling K 1963 *Phys. Rev. Lett.* **10** 516
Mandelshtam V A, Ravuri T R, and Taylor H S 1993 *Phys. Rev. Lett.* **70** 1932
Müller J, Burgdörfer J, and Noid D 1992 *Phys. Rev.* A **45** 1471
Müller J, Yang X, and Burgdörfer J 1994 *Phys. Rev.* A **49** 2470
Oza D H 1986 *Phys. Rev.* A **33** 824
Pekeris C L 1958 *Phys. Rev.* **112** 549
Pont M and Shakeshaft R 1995 *Phys. Rev.* A **51** 257
Reinhardt W P 1982 *An. Rev. Phys. Chem.* **33** 223
Richter K, Briggs J S, Wintgen D and Solov'ev E A 1992 *J. Phys. B: At. Mol. Opt. Phys.* **25** 3929
Richter K and Wintgen D 1991 *J. Phys. B: At. Mol. Opt. Phys.* **24** L565
Rost J M and Briggs J S 1990 *J. Phys. B: At. Mol. Opt. Phys.* **23** L339
——1991 *J. Phys. B: At. Mol. Opt. Phys.* **24** 4293
Rost J M, Gersbacher R, Richter K, Wintgen D and Briggs J S 1991 *J. Phys. B: At. Mol. Opt. Phys.* **24** 2455
Sadeghpour H R 1991 *Phys. Rev.* A **43** 5821

Salomonson S and Öster P 1989 *Phys. Rev.* A **40** 5559
Seaton M J 1983 *Rep. Prog. Phys.* **46** 167
Tang J, Watanabe S, and Matsuzawa M 1992 *Phys. Rev.* A **46** 2437
Wintgen D, Bürgers A, Richter K and Tanner G 1994 *Prog. Theor. Phys. Suppl.* **116** 121
Wintgen D and Delande D 1993 *J. Phys. B: At. Mol. Opt. Phys.* **26** L399
Wintgen D and Friedrich H 1987 *Phys. Rev.* A **35** 1628